A Novel CSI-Fed Induction Motor Drive

Abdul Rahiman Beig, *Member, IEEE*, and V. T. Ranganathan, *Senior Member, IEEE*

***Abstract*—Current source inverter (CSI) fed drives are employed in high power applications. The conventional CSI drives suffer from drawbacks such as harmonic resonance, unstable operation at low speed ranges, and torque pulsation. This paper presents a novel CSI drive which overcomes all these drawbacks and results in sinusoidal motor voltage and current even with CSI switching at fundamental frequency. The proposed CSI drive uses a three-level inverter as an active filter across motor terminals replacing the bulky ac capacitors used in the conventional drive. A sensorless vector controlled CSI drive based on proposed configuration is developed. The simulation and experimental results are presented. Experimental results show that the proposed drive has stable operation even at low speeds. Comparative results show that the proposed CSI drive has improved torque ripple compared to the conventional configuration.**

***Index Terms*—Active filters, current control, current source inverters (CSI), harmonic distortion, induction motor drives, multilevel inverters, pulsewidth modulation (PWM).**

I. Introduction

EVEN though voltage source inverter (VSI)-fed drives are most widely used, current source inverter (CSI)-fed drives find application in high power drives such as fan drives, where fast dynamic response is not needed, because of the following advantages.

- Inherent four quadrant operation:
  CSI drives employ fully controlled silicon-controlled rectifier (SCR) converters at the input. Under regeneration the polarity of the voltage at the converter terminals will reverse and the energy will be fed back to the utility. So regeneration is built into the system and unlike VSI fed drives, does not require an additional circuit
- Reliability:
  The dc link reactor will limit the rate of rise of current under short circuit. So the drives can be easily protected under short circuit. This results in improved reliability of the drive.

The presence of dc link reactor will result in slow dynamic response of the drive, hence these drives are used where fast dynamic response is not needed.

Fig. 1 shows the functional block diagram of the conventional CSI drive. The present day CSI drives employ self commutating devices such as gate turn-off thyristors (GTOs) instead of SCRs as in the past. Pulsewidth modulation (PWM) techniques can be used to get improved output current and voltage. Even

Manuscript received July 27, 2004; revised April 28, 2005. Recommended by Associate Editor A. M. Trzynadlowski.

A. R. Beig is with the Department of Electrical and Electronics Engineering, National Institute of Technology, Karnataka 575025, India (e-mail: arbeig@ieee.org).

V. T. Ranganathan is with the Department of Electrical Engineering, Indian Institute of Science, Bangalore, India (e-mail: vtran@ee.iisc.ernet.in).

Digital Object Identifier 10.1109/TPEL.2006.876826

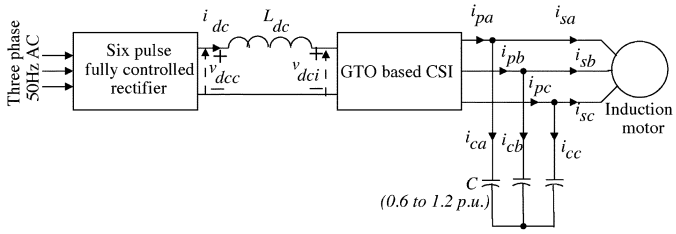

Fig. 1. Functional block diagram of conventional CSI fed drive.

though a relatively high switching frequency PWM will result in near sinusoidal output voltages and currents, at higher power levels, the CSI is switched at low frequency, ($f_{\rm sw}$ <200 Hz), to reduce switching losses. Reference [1] describes a conventional CSI drive, which employs selective harmonic elimination PWM technique, that results in acceptable waveform quality at low switching frequency. The conventional drives employ bulky ac capacitors across the motor terminals to control the voltage stress caused due fast changes in motor current during CSI switching. The presence of these capacitors results in resonance problem [2]. There are two modes of resonance. They are i) harmonic frequency resonance and ii) fundamental frequency resonance. The fundamental frequency resonance is due to the magnetizing inductance of the motor and the capacitor. This puts an upper limit on the value of C.So $C_{\max}$, the maximum value of C, is chosen such that the following constraint is satisfied

$$f_{1\rm res} = \frac{1}{2\pi\sqrt{L_o C_{\max}}} > F_{s\,\max}, \tag{1}$$

where L_o is the magnetizing inductance of the motor and $F_{s\,\max}$ is the maximum value of fundamental frequency, F_s. A relatively low value of C will result in poor filtering action and hence torque pulsations will be high. Typical values of C range from 0.6 p.u. to 1.2 p.u. depending on the value of L_o and $F_{s\,\max}$.

The harmonic resonance is mainly due to the leakage inductance and the capacitor; the resonance frequency is given by $f_{\rm hres} = (1)/(2\pi)(1)/(\sqrt{L_h C})$, where $L_h = L_{ls} + (L_{lr}||L_o)$, L_{ls} and L_{lr} are the stator and rotor leakage inductance, respectively. The resonance frequency will be exited if a harmonic of order h exists in the inverter output current that has a fundamental frequency at or near $F_s = (f_{\rm hres})/(h)$. Selective harmonic elimination techniques are invariably used to ensure that for a given fundamental frequency, the harmonic frequency corresponding to the resonance condition is avoided. At low modulation indices, the number of pulses, P becomes too large, hence trapezoidal PWM technique is employed [2]. The attenuation of harmonics in trapezoidal PWM is a function of P and modulation index M_i. So the value of P and M_i have to be carefully selected depending on the motor parameters and

value of C. But it is not possible to completely avoid resonance at low values of F_s. To overcome this problem, CSI drives are accelerated at rapid rate [3].

Even though capacitors help in attenuating voltage spikes during commutation of the CSI devices, their filtering action is poor. So there will be considerable amount of lower order harmonics in the motor current especially at low speed ranges and this will cause torque pulsation and increased harmonic losses in the motor. So the performance of the CSI drives is poor at low speed ranges. In summary it can be said that the CSI suffers from some of the major drawbacks such as harmonic losses in motor, harmonic torque pulsation, resonance problem, unstable operation at low speeds.

This paper proposes a novel CSI fed induction motor drive in which the VSI is used as an active filter across the motor terminals. The proposed configuration not only overcomes most of the drawbacks of conventional CSI drive but also ensures sinusoidal motor voltage and current waveforms throughout the operating range of the drive. The proposed CSI drive has significant differences compared to the similar drive schemes published in [4]–[6]. In the tandem or hybrid inverter scheme given in [4], [5], the VSI is directly connected to the motor terminals. In this case, the role of VSI is that of a voltage clamp rather than a harmonic filter. The motor voltages will still be PWM in nature and the associated problems such as stress on insulation, reflections due to long cables, etc. will remain. It is also difficult to cater to higher motor voltages. [6] describes a scheme in which the VSI is envisaged as a harmonic filter as well as a source of reactive power to commutate the CSI. However, the VSI is operated in the v/f mode without any current control. Also, the output filter capacitors required are quite large, approaching the output capacitors of a conventional GTO based CSI drive.

The proposed CSI drive configuration is explained in Section II. A sensorless vector control drive based on proposed CSI configuration is presented in Section III. Sensorless vector controlled drives based on both the conventional CSI configuration and proposed CSI configuration are simulated and the simulation results are presented in Section IV. The proposed drive is implemented on an experimental prototype. The experimental results are presented in Section V. From these results it can be concluded that the proposed drive has superior performance over conventional CSI drives in terms of improved motor current and voltage waveforms, reduced switching losses in CSI and stable operation in low speed ranges.

II. Novel CSI-Fed Induction Motor Drive

Active filters are successfully used in utility applications to filter out the harmonics from the supply currents. Active filters result in better performance compared to passive filters [7], [8]. In the proposed drive, active filters are used instead of capacitors across the induction motor as shown in Fig. 2. Unlike capacitors, the active filter serves dual purpose, that is the active filter not only limits the voltage surge caused due to the fast change in motor current during CSI switchings but also filters out harmonics effectively from the CSI current. Since the active filter has to carry only the harmonic currents, the rating of the filter needs to be only 25% to 30% of the rating of the drive. Therefore an IGBT based inverter can be used, which will result in high bandwidth. For a given bandwidth, the active filter effectively eliminates the harmonics which are within its bandwidth. Hence, the CSI can be switched at fundamental frequency and the switching losses can be reduced. Also the design of the power circuit becomes simple. Generally CSI drives of high rating operate at medium voltage ranges, so multilevel inverters are suitable for the active filter compared to the conventional two level inverter. For a given switching frequency, the M-level inverter will have a bandwidth equal to $(M-1)$ times the bandwidth of conventional two level inverters. Since only harmonic power has to be exchanged, the dc link capacitor voltage balancing problem will not be significant [9]. Hence diode clamp inverters are suitable for this type of application. In the present work, a three level diode clamp VSI is used as active filter. Fig. 2 shows the functional block diagram of the proposed CSI-fed drive. Vector control algorithm is implemented on the proposed drive configuration. The detailed power circuit and various controller blocks are shown in Fig. 3. Design of various controllers, generation of reference for active filter current controllers, synchronization of active filter and CSI are explained in the following sections.

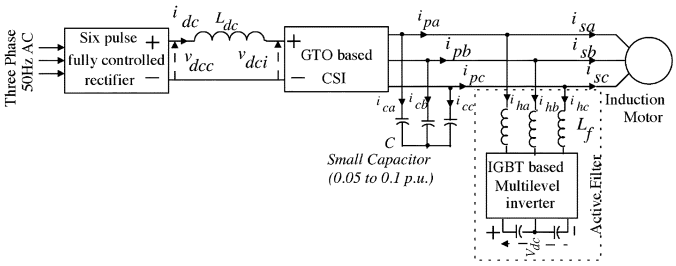

Fig. 2. Functional block diagram of proposed CSI fed drive.

A. Design of Active Filter Current Controllers

The active filter is modelled as follows:

$$\bar{v}_s(t) = R_f \bar{i}_h(t) + L_f \frac{d[\bar{i}_h(t)]}{dt} + \bar{v}_f, \tag{2}$$

where $\bar{v}_s, \bar{i}_h$ and $\bar{v}_f$ are the space vectors representing the motor terminal voltage, active filter current and active filter output voltage, respectively. The α and β components of (2), are given by

$$v_{s\alpha}(t) = R_f i_{h\alpha}(t) + L_f \frac{d[i_{h\alpha}(t)]}{dt} + v_{f\alpha} \tag{3a}$$

$$v_{s\beta}(t) = R_f i_{h\beta}(t) + L_f \frac{d[i_{h\beta}(t)]}{dt} + v_{f\beta}. \tag{3b}$$

The effect of motor voltages is compensated using feed forward technique as shown in Fig. 3. The filter current control is done in stationary coordinates, since the filter does not produce fundamental current. Using P–I controllers, defined in (4), a fast dynamic response can be achieved

$$k_{\mathrm{pf}}(i^*_{h\alpha}(t) - i_{h\alpha}(t)) + K_{\mathrm{if}} \int [(i^*_{h\alpha}(t) - i_{h\alpha}(t)]dt = v_{fs\alpha}(t) \tag{4a}$$

$$k_{\mathrm{pf}}(i^*_{h\beta}(t) - i_{h\beta}(t)) + K_{\mathrm{if}} \int [(i^*_{h\beta}(t) - i_{h\beta}(t))]dt = v_{fs\beta}(t) \tag{4b}$$

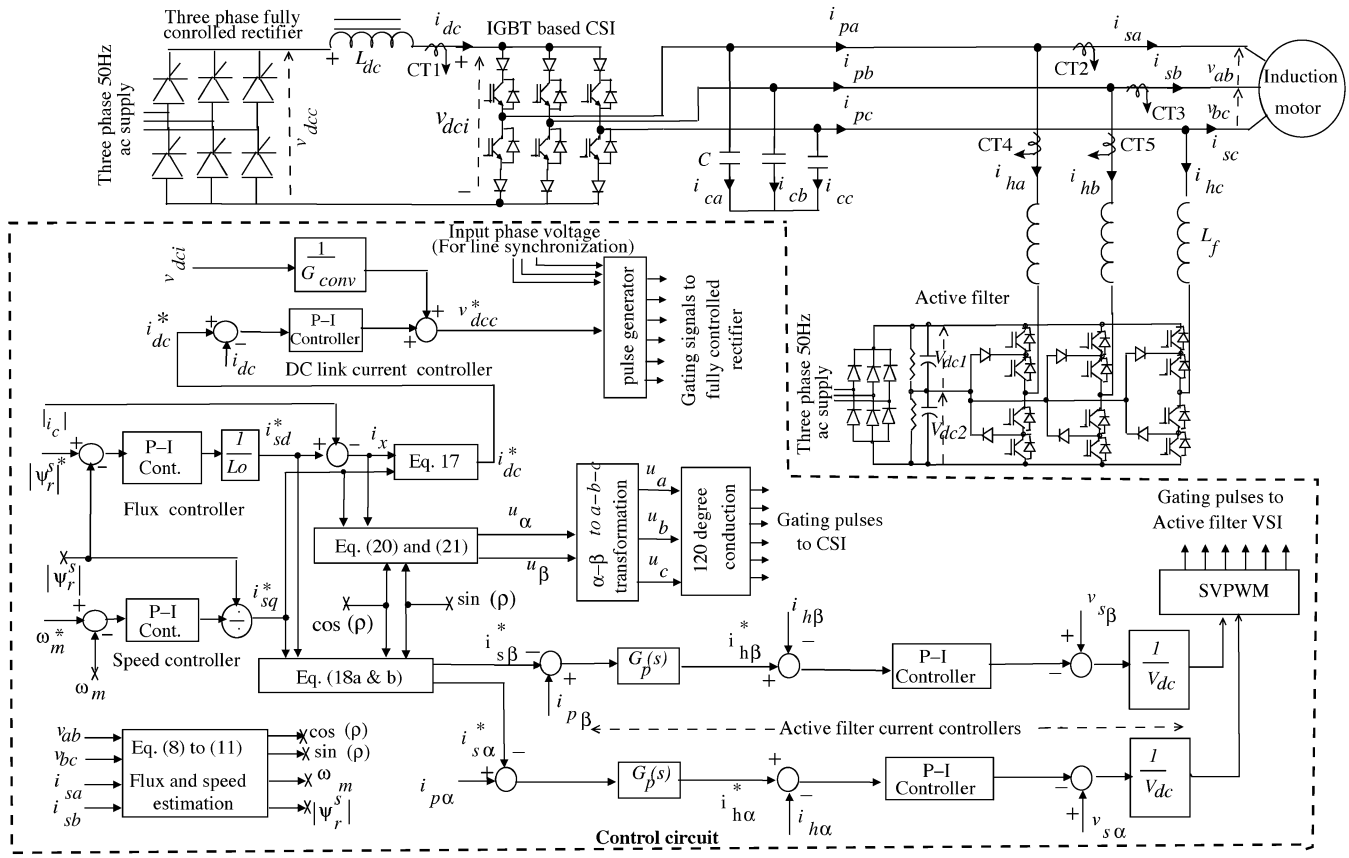

Fig. 3. Functional block diagram of vector control CSI drive based on proposed configuration.

where $v_{fs\alpha}(t) = v_{s\alpha}(t) - v_{f\alpha}(t)$ and $v_{fs\beta}(t) = v_{s\beta}(t) - v_{f\beta}(t)$. Neglecting the time constant of inverter τ_i, the closed loop transfer function of the current loop is given by

$$\frac{i_{h\alpha}}{i^*_{h\alpha}} = \frac{i_{h\beta}}{i^*_{h\beta}} = \frac{K_{\rm if}}{L_f} \frac{1 + s(k_{\rm pf}/K_{\rm if})}{s^2 + \frac{(R_f + k_{\rm pf})}{L_f} s + \frac{K_{\rm if}}{L_f}}. \tag{5}$$

In order to limit the overshoot a pre-filter $G_p(s) = (1)/(1 + (k_{\rm pf}/K_{\rm if})s)$ is used. The current loop has transfer function of second order with no zero; hence $k_{\rm pf}$ and $K_{\rm if}$ are selected based on the following design equations:

$$k_{\rm pf} = 2\zeta\omega_{ni}L_f - R_f \quad \text{and} \quad K_{\rm if} = L_f\omega^2_{ni} \tag{6}$$

where ω_{ni} is the bandwidth of the closed loop system.

In order to simplify the design of active filter circuit, the dc voltage is derived from the separate three phase supply and held constant at $V_{\rm dc}$. Modelling the three level inverter as a pure gain block with gain equal to $V_{\rm dc}$, the control inputs to the space vector block can be obtained using

$$v_{r\alpha} = \frac{v^*_{f\alpha}}{V_{\rm dc}} \quad \text{and} \quad v_{r\beta} = \frac{v^*_{f\beta}}{V_{\rm dc}}. \tag{7}$$

The space vector PWM is employed for active filter. The dc bus voltage, $V_{\rm dc}$ is selected such that the inputs $v_{r\alpha}$ and $v_{r\beta}$ are within the linear range of the modulation.

B. Active Filter Inverter and PWM Technique

CSI drives generally operate at medium voltage levels. So multilevel inverters are more suitable. In the proposed drive a three level diode clamp inverter is used. Since the inverter has to supply only harmonic currents, there is no capacitor voltage imbalance problem [9]. The rating of the active filter inverter is about 25% to 30% of the rating of the drive. Hence IGBTs can be used and inverters can be switched at high frequency. A simplified symmetrical three level space vector PWM technique [10] is employed. Any other three level PWM technique such as sine triangle PWM can also be used.

C. Switching Frequency of CSI

Since the active filter can suppress all the harmonics up to desired order, the CSI can be switched at fundamental frequency and switching loss will be reduced. So slow devices like GTO can be used for the CSI. In the present work IGBTs with series diodes are used for CSI. A simple switching pattern like 120° conduction with fundamental frequency switching is used.

III. Sensorless Vector Control of CSI Fed Induction Motor Drive

Since CSI drives cannot work on open loop, a sensorless vector controlled scheme for the proposed CSI drive configuration is employed. The functional block diagram of the sensorless vector controlled drive is shown in Fig. 3.

A. Rotor Flux Position Estimation

The vector control algorithm requires rotor flux position ρ, which can be estimated from the motor model [11], [12]. The stator flux space vector, $\bar{\psi}_s^s(t)$, is estimated using

$$\bar{\psi}_s^s(t) = \int (\bar{v}_s^s(t) - R_s \bar{i}_s^s(t))dt \tag{8}$$

where $\bar{v}_s(t)$ and $\bar{i}_s(t)$ are the stator voltage and current space vectors. Superscript ^{s} indicates that the variables are referred to stator axis.

The rotor flux vector, $\bar{\psi}_r^s(t)$ is obtained by subtracting the leakage flux from the stator flux vector as in

$$\bar{\psi}_r^s(t) = \frac{L_r}{L_o}(\bar{\psi}_s^s(t) - \sigma L_s \bar{i}_s^s(t)) \tag{9}$$

where L_s, L_r, and L_o, are the stator self inductance, rotor self inductance, and magnetizing inductance, respectively. The leakage factor σ is defined as $\sigma = 1 - (L_o^2)/(L_s L_r)$.

From the rotor flux vector the unit vectors of rotor flux position $\cos(\rho)$ and $\sin(\rho)$ can be obtained using

$$\cos(\rho) = \frac{\psi_{r\alpha}^s(t)}{|\bar{\psi}_r^s|} \quad \text{and} \quad \sin(\rho) = \frac{\psi_{r\beta}^s(t)}{|\bar{\psi}_r^s|}. \tag{10}$$

B. Speed Estimation

From the unit vectors, $\cos(\rho)$ and $\sin(\rho)$, the synchronous speed ω_s is obtained using

$$\omega_s = \frac{d\rho}{dt} = \cos(\rho)\frac{d(\sin(\rho))}{dt} - \sin(\rho)\frac{d(\cos(\rho))}{dt}. \tag{11}$$

The motor speed is estimated using $\omega_m(t) = \omega_s(t) - \omega_{\text{slip}}(t)$ and the slip frequency is given by $\omega_{\text{slip}}(t) = (i_{sq}(t))/(T_r i_{mr}(t))$. The d-axis and q-axis components of stator currents $i_{sd}(t)$ and $i_{sq}(t)$ are obtained from $i_{s\alpha}(t)$ and $i_{s\beta}(t)$using $\alpha - \beta$ to d–q transformation.

The magnetizing current of the rotor flux, $i_{mr}(t)$ is computed using $i_{mr}(t) = (\psi_{rd})/(L_o) = (|\bar{\psi}_r^s(t)|)/(L_o)$.

C. DC Link Current Controller

The line side converter is an SCR based fully controlled three-phase rectifier. A reactor is used to smoothen the dc link current and this forms the constant current source. The dc link current dynamics can be modelled as

$$v_{\text{dcc}}(t) = R_{\text{dc}} i_{\text{dc}}(t) + L_{\text{dc}}\frac{di_{\text{dc}}(t)}{dt} + v_{\text{dci}}(t) \tag{12}$$

where v_{dcc} is the converter output voltage, v_{dci} is voltage across CSI dc bus, R_{dc} is the resistance of the dc link reactor and L_{dc} is the inductance of the dc link reactor. The average value of v_{dcc} is related to the firing angle α_{conv} as $V_{\text{dcc}} = (\sqrt{3}V_{\text{inm}})/(\pi)\cos(\alpha_{\text{conv}})$, where V_{inm} is the peak input phase voltage. The converter gain is given by, $G_{\text{conv}} = (\sqrt{3}V_{\text{inm}})/(\pi)$. The effect of v_{dci} can be compensated by feed forward technique. Using the P–I controller, with $k_{\text{idc}} = (R_{\text{dc}})/(L_{\text{dc}})$, the closed loop transfer function of the dc current controller is given by

$$G_{\text{idc}} = \frac{1}{1 + \left(\frac{L_{\text{dc}}}{k_{\text{pdc}} G_{\text{conv}}}\right)(s(1 + s\tau_{\text{conv}}))}. \tag{13}$$

D. Speed Controller

The speed controller generates the torque reference. The speed controller can be realized as a PI controller, as the system dynamics is of the first-order as shown in

$$J\frac{d\omega_m(t)}{dt} + B\omega_m(t) = m_d(t) - m_l(t) \tag{14}$$

where J and B are the motor inertia and friction coefficients, respectively. m_l is the load torque and m_d is the generated torque given by

$$m_d(t) = \left(\frac{2}{3}\right)\left(\frac{p}{2}\right)\left[\left(\frac{L_o}{1+\sigma_r}\right) i_{mr}(t) i_{sq}(t)\right] \tag{15}$$

where p is the number of poles.

E. Flux Controller

The d-axis current $i_{sd}(t)$ is responsible for establishing flux in the machine. The dynamics related to the magnetizing current $i_{mr}(t)$ and $i_{sd}(t)$ is given by

$$T_r\frac{di_{mr}(t)}{dt} + i_{mr}(t) = i_{sd}(t). \tag{16}$$

The above equation is first order and $i_{mr}(t)$ can be controlled using a PI controller. The rotor flux is given by $\psi_r^s(t) = L_o i_{mr}^s(t)$. The capacitor current i_c is along the direct axis and in phase opposition with i_{sd}. The effect of i_c is compensated by subtracting its magnitude from $i_{sd}(t)$. The d-axis component of the current, to be supplied from the inverter is given by $i_x = i_{sd}^* - |i_c|$. $|i_c|$ is proportional to F_s^2.

F. Estimation of Fundamental Components of Motor Currents

The reference to the dc link current controller is given by

$$i_{\text{dc}}^* = \sqrt{i_x^2 + i_{sq}^{*2}}. \tag{17}$$

The α and β components of the fundamental component of the motor current that is to be supplied by the CSI inverter is obtained by d–q to α–β transoformation of i_{sd}^* and i_{sq}^* as in

$$i_{s\alpha}^* = i_{sd}^*\cos(\rho) - i_{sq}^*\sin(\rho) \tag{18a}$$
$$i_{s\beta}^* = i_{sd}^*\sin(\rho) + i_{sq}^*\cos(\rho). \tag{18b}$$

G. Estimation of Current References $i_{h\alpha}^*$ and $i_{h\beta}^*$

The current references to the active filter current controller $i_{h\alpha}^*$ and $i_{h\beta}^*$, are generated by subtracting the fundamental components from the actual CSI currents as in

$$i_{h\alpha}^* = i_{p\alpha} - i_{s\alpha}^* \tag{19a}$$
$$i_{h\beta}^* = i_{p\beta} - i_{s\beta}^* \tag{19b}$$

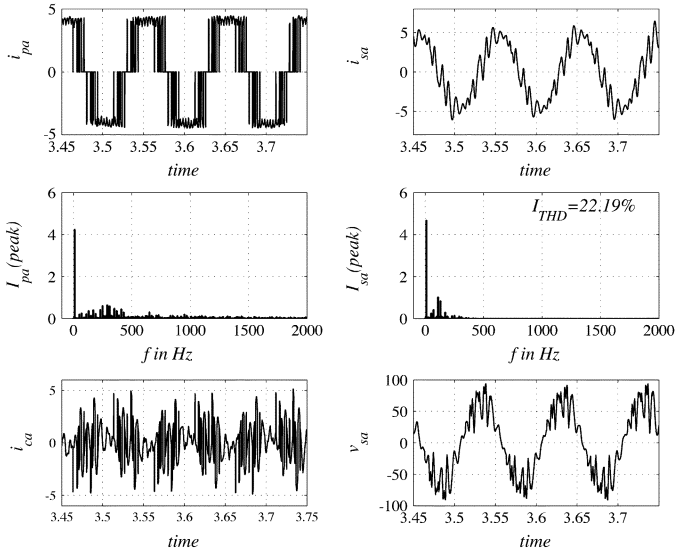

Fig. 4. Simulation results: Conventional drive, F_s =10 Hz, C =0.6 p.u., P = 18.

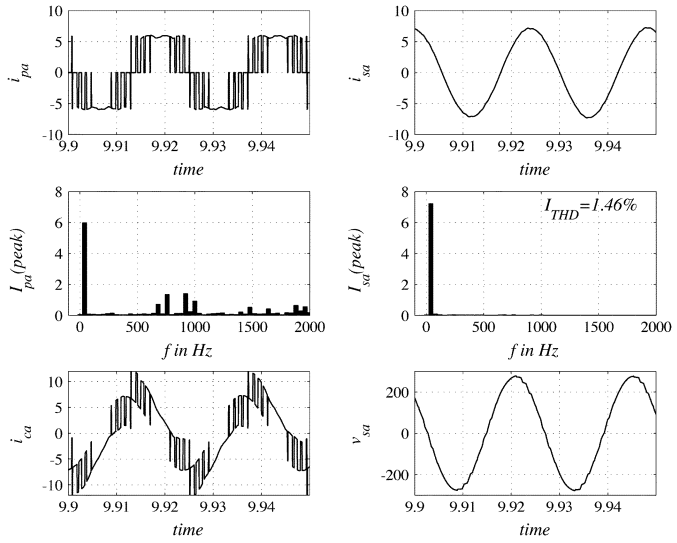

Fig. 5. Simulation results: Conventional drive, F_s = 40 Hz, C = 0.6 p.u., P =18.

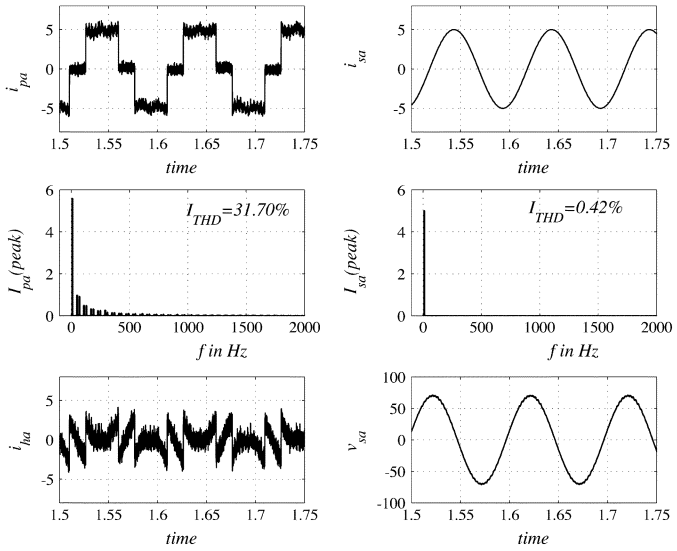

Fig. 6. Simulation results: Proposed drive F_s = 10 Hz [Case (i): High bandwidth (31416 rad./s)].

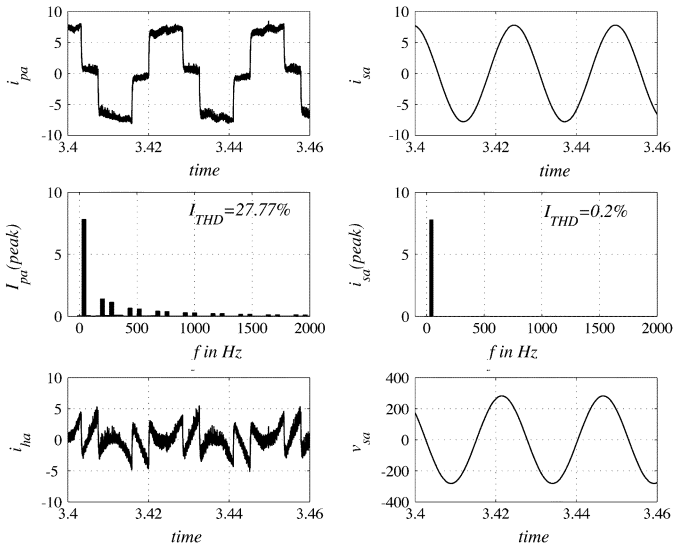

Fig. 7. Simulation results: Proposed drive F_s = 40 Hz [Case (i): High bandwidth (31416 rad./s)].

where $i_{p\alpha}$ and $i_{p\beta}$ are the α and β components of CSI current space vector.

H. Switching Pulses for CSI and Synchronization

The unit vectors along α–β axis are obtained by

$$u_\alpha = \frac{i^*_{d\alpha}}{|i_{\rm dc}|^*} \quad \text{and} \quad u_\beta = \frac{i^*_{d\beta}}{|i_{\rm dc}|^*} \tag{20}$$

where $i^*_{d\alpha}$ and $i^*_{d\beta}$ are obtained by d–q to α–β transformation of i_x and i^*_{sq} as in

$$i^*_{d\alpha} = i_x \cos(\rho) - i^*_{sq} \sin(\rho) \tag{21a}$$

$$i^*_{d\beta} = i_x \sin(\rho) + i^*_{sq} \cos(\rho). \tag{21b}$$

The three phase unit vectors are generated by transforming u_α and u_β to three phase quantities, i.e., a-b-c form. Using these unit vectors, the switching pulses for the CSI are generated. The switching pulses of active filter, switching pulses of CSI and the motor voltage are thus synchronized, so there is no need of a separate PLL circuit.

1) Need and Placement of Capacitor: The active filter current ripple at switching frequency will result in voltage ripple across the motor. So a small ac capacitor (<0.1 p.u.) is to be connected across the CSI terminals. It is preferred to connect these capacitors directly across the CSI than on the motor terminals because of the following advantages.

- It provides a low impedance path for the current ripple due to active filter switchings. Higher the switching frequency lower is the capacitor value.
- By placing the capacitor on the CSI terminal, the voltage spikes due to the energy trapped in the stray inductances during CSI switchings can be attenuated.

- By positioning the capacitors near the CSI terminals, any resonance between the capacitor and motor will be filtered out by the active filter.

IV. Simulation Results

The vector controlled drives based on both the conventional CSI and proposed CSI configuration are simulated using MATLAB-SIMULINK tool box. The rating and the parameters of the motor used in the simulation are given in the Appendix.

A. Simulation Results: Conventional CSI Drive

The vector controlled conventional CSI drive, described in [1] is simulated using MATLAB-SIMULINK tool box. Figs. 4 and 5 show the CSI current (i_{pa}), motor current (i_{sa}), capacitor current (i_{ca}), motor phase voltage (v_{sa}), harmonic spectra of i_{pa}, and i_{sa} as obtained from the simulation for $F_s = 10$ Hz and $F_s = 40$ Hz, respectively. Capacitor $C = 0.6$ p.u. (i.e., 66 μF) is used in simulation. In simulation, $P = 18$ is used for $F_s >$20 Hz, so that the fifth, seventh, 11th, and 13th are eliminated. The rating of the motor under consideration is given in Appendix. From the results it can be seen that at low F_s, the motor current and voltage have significant harmonics. The filtering action of the capacitor is good at higher values of F_s. But as F_s increases, the fundamental component of the capacitor current also increases; that means VA rating of the capacitor will rise with F_s.

B. Simulation Results: Proposed CSI Drive

The vector control scheme is applied to the proposed CSI drive and the system is simulated using MATLAB-SIMULINK tool box. Figs. 6 and 7 give the simulation results of i_{pa}, i_{sa}, their harmonic spectra, active filter current (i_{ha}) and v_{sa} for $F_s = 10$ Hz and $F_s = 40$ Hz, respectively. Small ac capacitors of 0.1 p.u. ($C = 11$ μF) are used to filter out the voltage due to active filter switching ripple. A high bandwidth of 31416 rad/s is used for the active filter. Comparing these results with the simulation results for the conventional drive (given in Figs. 4 and 7), the following observations can be made.

- Compared to the filtering action of capacitors in conventional drive, the filtering action of active filter is uniform for the entire range of the fundamental frequency of the drive. Hence, motor currents have improved THD. For example, from the simulation results we can see that for $F_s =$ 10 Hz, THD of motor current is 0.42% in the case of proposed drive and 22.19% for conventional drive. Similarly for $F_s = 40$ Hz, the THD is 0.2% for conventional drive and 1.42% for conventional drive.
- The active filter draws only harmonic currents, whereas the capacitor draws fundamental current also. The VA rating of active filter will be small.
- The $i_{\rm dc}$ has low frequency oscillation. This is because the dc link current controller is not responding fast enough to the variation in $v_{\rm dci}$. But the active filter is able to absorb these low frequency components of $i_{\rm dc}$. So in case of proposed drive, the tuning of the dc link current controller is easy.
- Since the capacitor in the conventional CSI drive supplies leading VAR, the current rating of the conventional CSI is less compared to that of proposed CSI drive.

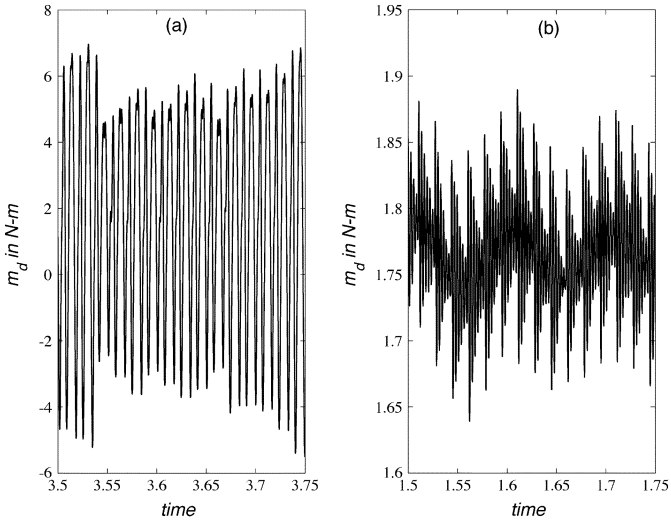

Fig. 8. Simulation results: m_d at steady state, $F_s = 10$ Hz: (a) conventional drive and (b) proposed drive.

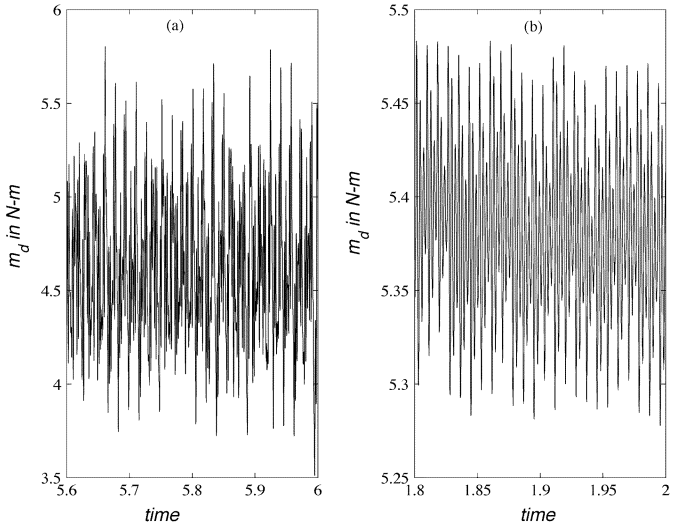

Fig. 9. Simulation results: m_d at steady state, $F_s = 20$ Hz: (a) conventional drive and (b) proposed drive.

- Since filtering action is better, the torque ripple is reduced in proposed CSI drive compared to the conventional drive. Comparative plots of the estimated torque at steady state for two operating conditions, $F_s = 10$ Hz and $F_s = 20$ Hz are given in Figs. 8 and 9, respectively.

V. Experimental Verification

The proposed drive is implemented on an experimental prototype. A six-pulse three-phase fully controlled SCR ac to dc converter is used on the line side. An IGBT based three-phase three-level diode clamp inverter is designed and fabricated in the laboratory and used as active filter inverter. An IGBT based CSI is designed and fabricated in the laboratory. Diodes are connected in series with the IGBT modules as shown in Fig. 3 to block the reverse current flow through IGBT body diodes. The input line side voltages are sensed using potential transformers and these signals are used for synchronization of SCR firing pulses for the line side ac to dc converter. The voltage signals

namely active filter dc bus voltages $V_{\rm dc1}, V_{\rm dc2}, V_{\rm dci}$, motor terminal line voltages v_{ab} and v_{bc} are sensed using voltage sensing circuits designed in the laboratory, which make use of HPCL 7800 isolation amplifier. The placement of these transducers are shown by dotted arrow lines in Fig. 3. The motor phase voltages v_{sa} and v_{sb} cannot be measured directly so these are computed using line voltages across motor terminals v_{ab} and v_{bc}. The active filter dc bus voltage is maintained constant in the experimental set up as explained in Section II-A, but it is required for protection purpose. The currents $i_{\rm dc}, i_{sa}$, i_{sb}, i_{ha}, and i_{hb} are sensed using LEM make hall sensor CTs, CT1, CT2, CT3, CT4, and CT5, respectively. The placement of these hall sensor CTs are shown in Fig. 3. A single TMS320F240 DSP based controller, which is designed and developed in the laboratory is used to acquire the input signals, implement the control algorithm and to generate firing pulses to the active filter, CSI and the input rectifier. The digital controller has two limitations as listed below.

- The on chip ADC of the TMS320C240 is slow and requires about 6.6 μs per channel for data conversion.
- The controller board employs slow external memory, requires wait states to be inserted.

Due to these limitations and also the fact that a single DSP is doing the entire task, the total loop time of the algorithms is about 212 μs and hence the sampling time is set at 250 μs. The switching frequency of the active filter is chosen at 2 KHz. Hence, the bandwidth of the active filter current controller is set at 1 KHz. The rating of the active filter, CSI, and the various controller parameters are listed in the Appendix.

A. Selection of Active Filter Inductance

The active filter should be in a position to supply the high di/dt demanded by the CSI during switchings. The active filter inductance and bandwidth should be selected to satisfy this. Simulation results show that the active filter with sufficient bandwidth will be in a position to supply the di/dt as demanded by the CSI and hence suppresses all the high frequency harmonics of the CSI currents. However, from the experiments it is observed that if the active filter bandwidth is low, the active filter will not be in a position to suppress the high frequency harmonics and the uncompensated energy triggers resonance between active filter inductance and capacitor. In order to attenuate this resonance, the inductor is selected such that the resonance frequency is above the bandwidth of the active filter. In the experimental prototype, $L_f = 0.5$ mH and this value will be enough to supply the di/dt demanded by the CSI and also push resonance frequency above the bandwidth of the active filter.

B. Design of Active Filter Current Controllers With Low Bandwidth

In the experimental setup, the bandwidth of the active filter is selected to be 6283 rad/s. The low bandwidth of the active filter will result in phase lag for frequencies in the pass band. So the filtering action is not perfect. The phase lag problem is overcome by introducing lead-lag compensators for the current references.

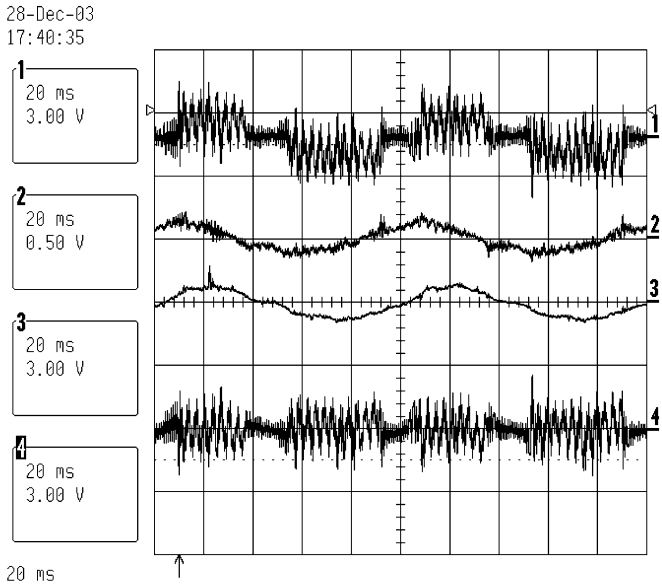

Fig. 10. Experimental results: Steady state current and voltage waveform, $F_s = 10$ Hz. Ch1: i_{pa} (6.66 A/div), Ch2: v_{ab} (250 V/div), Ch3: i_{sa} (6.66 A/div) and Ch4: i_{ha} (6.66 A/div).

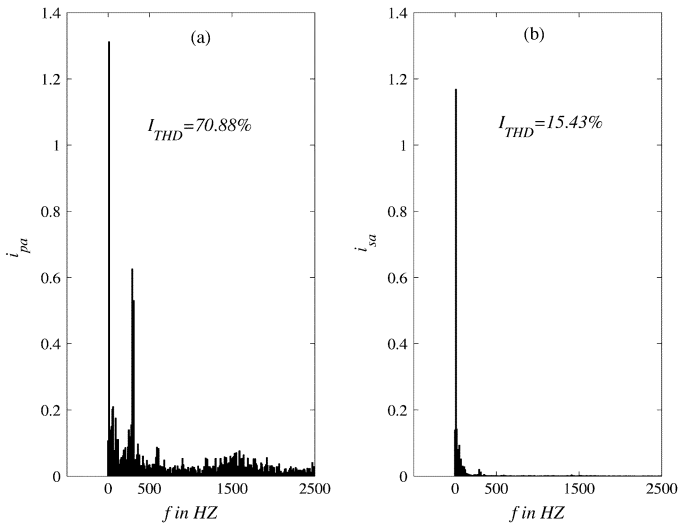

Fig. 11. Experimental results: Harmonic spectra of (a) i_{pa} and (b) i_{sa} at $F_s = 10$ Hz.

C. Experimental Results

The loading arrangement in the experimental prototype consists of a separately excited shunt dc generator, coupled to the induction motor. The ratings of these motors are given in Appendix. In this type of loading, torque is proportional to speed, whereas the actual load encountered by CSI drives is of the fan type load in which the torque is proportional to square of the speed. The above induction motor is connected in star, so the flux in the machine is $(1/\sqrt{3})$ of the rated value and the torque developed is $(1/3)$ of the rated value [13]–[15].

Figs. 10 and 12 show the steady state experimental waveforms of i_{pa}, line voltage v_{ab}, i_{sa}, i_{ha}, for $F_s = 10$ Hz and $F_s = 40$ Hz, respectively. The harmonic spectra of i_{pa} and i_{sa}

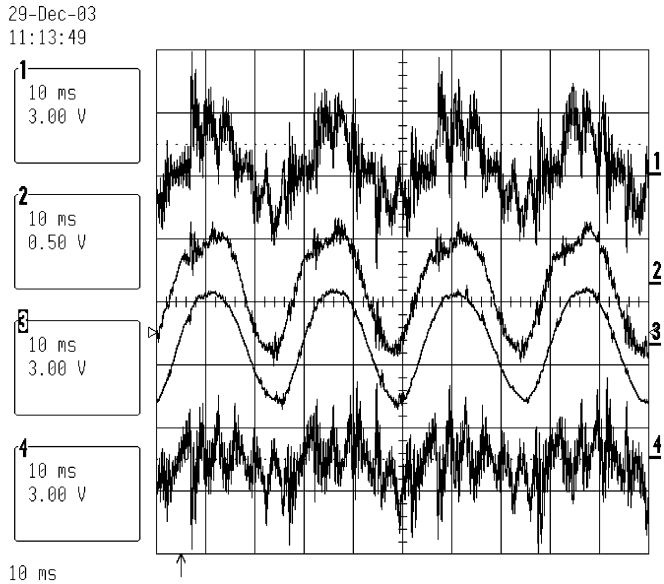

Fig. 12. Experimental results: Steady state current and voltage waveform, $F_s = 40$ Hz. Ch1: i_{pa} (6.66 A/div), Ch2: v_{ab} (250 V/div), Ch3: i_{sa} (6.66 A/div) and Ch4: i_{ha} (6.66 A/div).

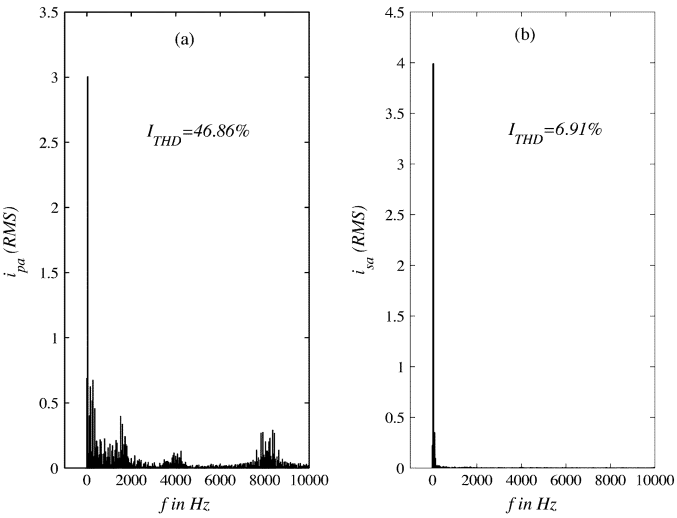

Fig. 13. Experimental results: Harmonic spectra of (a) i_{pa} and (b) i_{sa} at $F_s = 40$ Hz.

for $F_s = 10$ Hz and $F_s = 40$ Hz are given in Figs. 11 and 13, respectively.

Fig. 14 shows the variation of i_{sa} during speed reversal. In Fig. 14, trace A shows the variation of current during zero crossing of speed. From these results it is observed that the filtering action is maintained even near zero speed and the speed reversal is smooth.

D. Validation of the Model for Low Bandwidth Conditions

In order to verify the experimental results with the low bandwidth of the current controller (bandwidth = 6283 rad./s), the simulation is carried out under similar conditions. The simulation results with low bandwidth conditions for $F_s = 10$ Hz and $F_s = 40$ Hz are given in Figs. 15 and 16, respectively. The simulation results match with the experimental results given in Figs. 10–13.

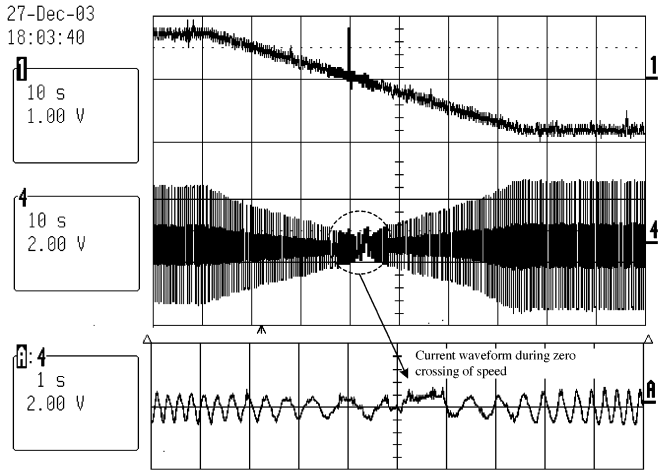

Fig. 14. Experimental results: Ch1: ω_m (Scale: 122 rad/s/div) Ch4: i_{sa} (4.44 A/div) ChA: time magnification of Ch4:(variation of i_{sa} during zero crossing of speed. Scale:(4.44 A/div).

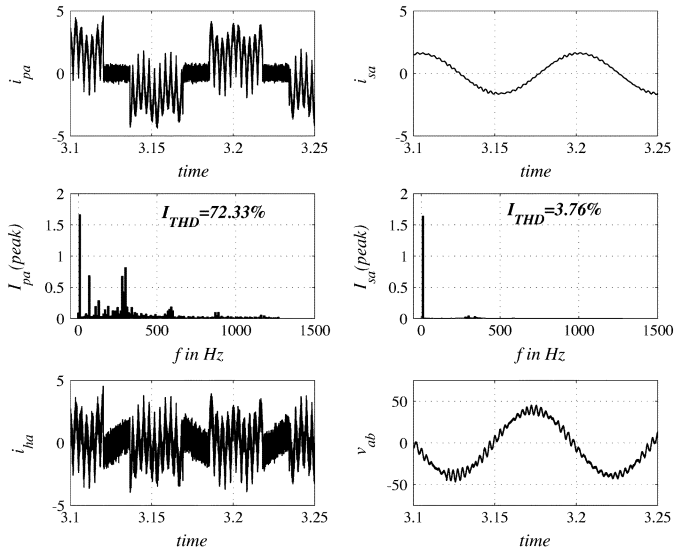

Fig. 15. Simulation results: Proposed drive $F_s = 10$ Hz (Case (ii) Low bandwidth = 6283 rad/s).

VI. Discussions

The following observations can be made from the above results.

- The dc link current $i_{\rm dc}$, has significant amount of ripple at 300 Hz. Because of this, i_{pa} has 300-Hz ripple. The harmonic spectrum of i_{pa} shows that it has predominantly low order harmonics and most of the harmonics are within the 1-KHz range. The active filter is able to filter out these harmonics; this results in near sinusoidal motor current with improved THD.
- It is observed that the filtering action is not complete with the limited bandwidth of the active filter current loops. This results in ripple component in motor voltages. The simulation results show that this problem is eliminated completely and motor current and voltage waveforms are sinusoidal when the active filter current controller bandwidth is high. It should be noted that, as explained in Section V, the experimental set up has low bandwidth due to the limitations

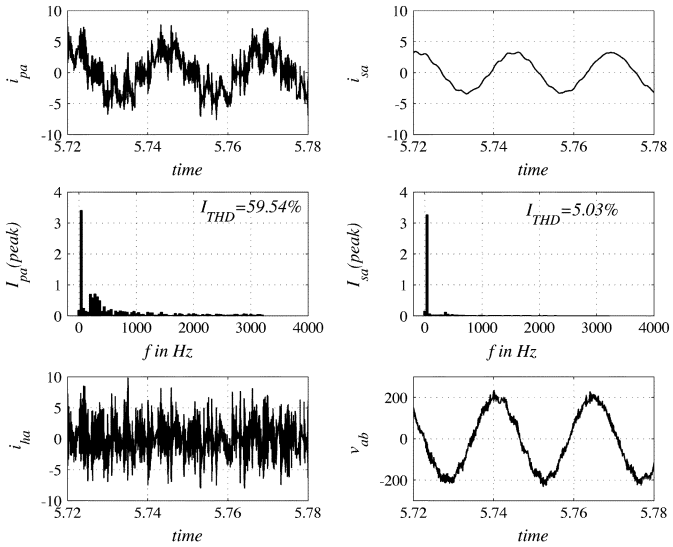

Fig. 16. Simulation results: Proposed drive $F_s = 40$ Hz (Case ii) low bandwidth = 6283 rad/s).

of the controller and not the inverter. Since the active filter inverter has to supply only the harmonic power, it is possible to achieve required high bandwidth by increasing the switching frequency if the controller is fast enough.

- There is low frequency distortion in motor current and voltage especially at low values of F_s. This is due to the improper tuning of the speed and flux controller. The difficulty in tuning these controller may be due to following reasons.
  - — Present work employs simple algorithm of estimating the flux by integrating the back emf. This method will result in errors at low speeds due to the effect of R_s. Also the dc offset in sensed signals of motor voltage and current may lead to error in flux estimation. This in turn will result in error in estimated value of rotor flux position signal ρ. Since unit vectors are generated based on ρ, the estimation of fundamental current of the CSI output current, estimation of harmonics in CSI output current and tuning of the flux and speed controller becomes difficult.
  - — The error in unit vectors will result in imbalance in the switching of the CSI. This in turn will contribute for the offset in motor currents.

    The above problem can be overcome by using improved algorithms for flux estimation such as those given in [3], [16], and [17]. These algorithms are more involved and since the focus of the present work is to demonstrate the CSI drive, only the simple method is used.
- Satisfactory steady state operation is achieved in the speed range 5 Hz to base frequency 50 Hz. With improved flux estimation algorithms it may be possible to achieve satisfactory performance even at near zero speeds. However speed reversal is smooth without any difficulty near zero speed.
- At low bandwidth conditions, it becomes difficult to tune the flux controller. Improper tuning of the flux controller results in variation in $i_{\rm dc}$, which in turn results in error in the estimation of fundamental components of motor current. The error in estimation of fundamental components will make the active filter supply fundamental component. However, from the simulation it is observed that no such problems are faced under high bandwidth of active filter current controllers.

TABLE I
EXPERIMENTAL DRIVE: RATINGS

Induction motor:	400V, 8A, 3.78 KW, 1425rpm, 3ϕ, 50Hz
DC machine:	230V,13A, 3KW, 1475rpm, Filed: 230V,1.1A.
Input rectifier:	3ϕ, six pulse SCR based.
Input voltage:	415V, 50Hz, 3ϕ ac supply.
CSI:	3ϕ IGBT based.
DC input voltage:	700V Max..
DC link current:	50A Max..
Active filter:	3ϕ three level IGBT based DCI.
DC bus voltage:	600V (nominal)
DC bus current:	50A Max.
Speed range:	5Hz to base frequency 50Hz.

TABLE II
EXPERIMENTAL DRIVE: PARAMETERS

Parameter	Value	Parameter	Value
R_s	1.5313Ω	R_r	1.5313Ω
L_{ls}	0.0094 H	L_{lr}	0.0094 H
L_s	0.2194 H	L_r	0.2194 H
L_o	0.2100 H	J	0.25 Kg_m^2
p	4	B	$0.025Kg\_m^2/sec$
ψ_{Rated}	1.555 wb	L_{dc}	$42mH$
m_{dRated}	25.33 N_m	R_{dc}	1.06Ω
k_{pdc}	$0.0396/A$	k_{idc}	$25.26rad/sec$
L_f	$0.5mH$	k_{pw}	$1N\_m.sec/rad$
R_f	0.15Ω	k_{if}	$300rad/sec$
k_{pf}	3.066Ω	k_{iw}	$0.0067rad.sec$
k_{pfr}	$0.1A/wb$	k_{ifr}	$7rad/sec$
C	$11\mu F$	v_{inm}	390V

VII. CONCLUSION

A novel CSI-fed induction motor drive with sinusoidal motor current and voltage waveforms is proposed. A vector controlled drive based on the proposed CSI configuration has been simulated and verified experimentally.

Excellent waveforms for the motor voltage and current can be obtained with sufficient bandwidth of the active filter current controller loops. In the experimental drive, because of the limitations of the DSP based controller used, the bandwidth of active filter current controllers is restricted to 6283 rad/s. Even with this low bandwidth, the active filter is able to filter out most of the low order harmonics and the resulting current and voltage waveforms are near sinusoidal.

Moreover compared to the conventional CSI drive, the proposed drive results in near sinusoidal motor current and voltage waveform in the entire speed range of the drive including low speed because of the uniform filtering action of the active filter.

Since motor voltage and current waveforms are sinusoidal, high voltage stress due to reflected waveforms in long cables

are avoided, hence conventional motors can be retrofitted with the proposed drive. Also, the common mode voltage problem is reduced.

The CSI is switched at fundamental frequency with simple switching logic. Hence, design of the power circuit is simple. Also, the power loss in the CSI will be reduced.

APPENDIX

See Tables I and II.

REFERENCES

[1] P. M. Espelage, J. M. Nowak, and L. H. Walker, "Symmetrical GTO current source inverter for wide speed range control of 2300 to 4160 Volt, 350 to 7000 Hp, induction motors," in *Proc. IEEE Ind. Appl. Soc. Annu. Meeting*, Pittsburgh, Oct. 2–7, 1988, vol. 1, pp. 302–307.

[2] B. Wu, S. B. Dewan, and G. R. Slemon, "PWM CSI inverter for induction motor drives," *IEEE Trans. Ind. Appl.*, vol. 28, no. 1, pp. 64–71, Jan./Feb. 1992.

[3] B. K. Bose, *Modern power electronics and AC drives*. Delhi, India: Pearson Education (Singapore) Pvt. Ltd., 2003, ch. 6 and 8.

[4] Trzynadlowski, N. Patriciu, F. Blaabjerg, and J. K. Pedersen, "A hybrid, current-source/voltage-source power inverter circuit," *IEEE Trans. Power Electron.*, vol. 16, no. 6, pp. 866–871, Nov. 2001.

[5] M. Imecs, A. M. Trzynadlowski, I. I. Incze, and C. Szabo, "Vector control schemes for tandem-converter fed induction motor drives," *IEEE Trans. Power Electron.*, vol. 20, no. 2, pp. 493–501, Mar. 2005.

[6] S. Kwak and H. A. Toliyat, "A hybrid solution for load commuted inverter fed induction motor drive," *IEEE Trans. Ind. Appl.*, vol. 41, no. 1, pp. 83–90, Jan./Feb. 2005.

[7] P. S Sensarma, K. R. Padiyar, and V. Ramanarayanan, "A comparative study of harmonic filtering strategies for a shunt active filter," in *Proc. IEEE IAS Annu. Meeting Conf.*, Rome, Italy, 2000, vol. 3, pp. 2509–2516.

[8] H. Akagi, "Trends in active power line condensers," *IEEE Trans. Power Electron.*, vol. 9, no. 3, pp. 263–268, May 1994.

[9] J.-S. Lai and F. Z. peng, "Multilevel converters—A new breed of power converters," *IEEE Trans. Ind. Appl.*, vol. IA-32, no. 3, pp. 509–517, May/Jun. 1996.

[10] A. R. Beig and V.T. Ranganathan, "Influence of placement of small space vectors on the performance of PWM techniques for three level inverters," in *Proc. IEEE Ind. Electron. Soc. (IECON'03)*, Roanoke, VA, Nov. 2–6, 2003, vol. 3, pp. 2764–2770.

[11] N. Mendalek and K. Al Haddad, "Modelling and non linear control of shunt active power filter in the synchronous reference frame," in *Proc. IEEE 9th Int. Conf. Harmonics Qual. Power*, Orlando, FL, Oct. 1–4, 2000, vol. 1, pp. 30–35.

[12] W. Leonhard, *Control of Electrical Drives*, 3rd ed. NewYork: Springer-Verlag, 2001, ch. 12.

[13] S. Bolognani and G. S. Bhuja, "DC link current control for high performance CSI Drives," *IEEE Trans. Ind. Appl.*, vol. IA-23, no. 6, pp. 1043–1047, Nov./Dec. 1987.

[14] N. Kas, M. Kamatani, and H. Watanabe, "Current source inverter drive speed sensor-less vector controlled induction motor," in *Proc. IEEE Int. Conf. Ind. Electron., Contr., Instrum.*, Nov. 15–19, 1993, vol. 2, pp. 983–986.

[15] "Novel High Performance CSI Fed Induction Motor Drive With Sinusoidal Motor Voltages and Currents," Indian Patent Application, Indian Institute of Science, 2004.

[16] J. Hu and B. Wu, "New integration algorithm for estimating motor flux over a wide speed range," *IEEE Tran. Power Electron.*, vol. 13, no. 5, pp. 969–977, Sep. 1998.

[17] C. Schauder, "Adaptive speed identification for vector control of induction motor without rotational transducers," *IEEE Trans. Ind. Appl.*, vol. 28, no. 5, pp. 1054–1061, Sep./Oct. 1992.

Abdul Rahiman Beig (M'92) received the B.E. degree in electrical and electronics engineering from the National Institute of Technology Karnataka, Suratkal, India, in 1989, and the M. Tech. and Ph.D. degrees in electrical engineering from Indian Institute of Science, Bangalore, in 1998 and 2004, respectively.

He is currently an Assistant Professor in the Department of Electrical Engineering, National Institute of Technology Karnataka, Suratkal, India. From 1989 to 1992, he was with M/S Kirloskar Electric Company, Ltd, Mysore, India, as R&D Engineer in the Drives Group. His research interests include ac drives, multi level inverters.

Dr. Beig received the 1998 L&T ISTE National Award for the best M.E. thesis in Electrical and Electronics Engineering from the Indian Society for Technical Education, India.

V. T. Ranganathan (SM'84) received the B.E. and M.E. degrees in electrical engineering from the Indian Institute of Science (I.I.Sc.), Bangalore, and the Ph.D. degree from Concordia University, Montreal, QC, Canada.

He joined the Electrical Engineering Department, I.I.Sc., in 1984, where he is currently a Professor. He has published several papers in the areas of vector control of ac drives, PWM techniques, split phase induction motor drives and rotor side control of slip ring induction motors. He is also a consultant to industry in the above areas and has participated in a number of projects. His research interests are in the area of power electronics and motor drives.

Dr. Ranganathan received the Prize Paper Award of the IEEE-IAS Static Power Converter Committee and the Tata Rao Prize of the Institution of Engineers, India. He is a Fellow of the Institution of Engineers, India and the Indian National Academy of Engineering.